

# Insights into the location and dynamics of the coolest X-ray emitting gas in clusters of galaxies

C. Pinto,<sup>1\*</sup> A. C. Fabian,<sup>1</sup> A. Ogorzalek,<sup>2,3</sup> I. Zhuravleva,<sup>2,3</sup> N. Werner,<sup>2,3</sup>  
J. Sanders,<sup>4</sup> Y.-Y. Zhang,<sup>5</sup> Liyi Gu,<sup>6</sup> J. de Plaa,<sup>6</sup> J. Ahoranta,<sup>7</sup> A. Finoguenov,<sup>7</sup>  
R. Johnstone,<sup>1</sup> R.E.A. Canning,<sup>2,3</sup>

<sup>1</sup>*Institute of Astronomy, Madingley Road, CB3 0HA Cambridge, United Kingdom*

<sup>2</sup>*Kavli Institute for Particle Astrophysics and Cosmology, Stanford University, 452 Lomita Mall, Stanford, CA 94305-4085, USA*

<sup>3</sup>*Department of Physics, Stanford University, 382 via Pueblo Mall, Stanford, CA 94305-4060, USA*

<sup>4</sup>*Max-Planck-Institut für extraterrestrische Physik, Giessenbachstrasse 1, 85748 Garching, Germany*

<sup>5</sup>*Argelander-Institut für Astronomie, Universität Bonn, Auf dem Hügel 71, 53121 Bonn, Germany*

<sup>6</sup>*SRON Netherlands Institute for Space Research, Sorbonnelaan 2, 3584 CA Utrecht, The Netherlands*

<sup>7</sup>*Department of Physics, University of Helsinki, 00014 Helsinki, Finland*

Accepted 2016 June 13. Received 2016 June 9; in original form 2016 April 29

## ABSTRACT

We extend our previous study of the cool gas responsible for the emission of O VII X-ray lines in the cores of clusters and groups of galaxies. This is the coolest X-ray emitting phase and connects the 10,000 K H  $\alpha$  emitting gas to the million degree phase, providing a useful tool to understand cooling in these objects. We study the location of the O VII gas and its connection to the intermediate Fe XVII and hotter O VIII phases. We use high-resolution X-ray grating spectra of elliptical galaxies with strong Fe XVII line emission and detect O VII in 11 of 24 objects. Comparing the O VII detection level and resonant scattering, which is sensitive to turbulence and temperature, suggests that O VII is preferably found in cooler objects, where the Fe XVII resonant line is suppressed due to resonant scattering, indicating subsonic turbulence. Although a larger sample of sources and further observations is needed to distinguish between effects from temperature and turbulence, our results are consistent with cooling being suppressed at high turbulence as predicted by models of AGN feedback, gas sloshing and galactic mergers. In some objects the O VII resonant-to-forbidden line ratio is decreased by either resonant scattering or charge-exchange boosting the forbidden line, as we show for NGC 4636. Charge-exchange indicates interaction between neutral and ionized gas phases. The Perseus cluster also shows a high Fe XVII forbidden-to-resonance line ratio, which can be explained with resonant scattering by low-turbulence cool gas in the line-of-sight.

**Key words:** Intergalactic medium – intracuster medium – cooling flows – charge exchange – resonant scattering – turbulence.

## 1 INTRODUCTION

The intracuster medium (ICM) embedded in the deep gravitational well of clusters of galaxies has a complex multi-temperature structure with different cospatial phases ranging from  $\sim 10^6$  to above  $10^8$  K. It is thought to contain most of the baryonic mass of the clusters and its density strongly increases in their cores where the radiative cooling time is less than 1 Gyr and therefore shorter than their age. In the absence of heating, this would imply the cooling of hun-

dreds of solar masses of gas per year below  $10^6$  K (Fabian 1994). The gas is expected to produce prominent emission lines from O VI in UV, peaking at  $T \sim 3 \times 10^5$  K, as well as O VII ( $T \sim 2 \times 10^6$  K) and Fe XVII ( $T \sim 6 \times 10^6$  K) in X-rays, suggesting that spectroscopy is a key to understand the cooling processes in clusters of galaxies. Evidence of weak O VI UV lines was found by Bregman et al. (2005, 2006) at levels of  $30 M_\odot \text{ yr}^{-1}$  or lower, significantly less than the predicted  $100 M_\odot \text{ yr}^{-1}$ . Fe XVII emission lines have been discovered, but with luminosities much lower than expected from cooling-flow models (see e.g. Peterson et al. 2003). O VII lines were detected for the first time in a stacked spectrum

\* E-mail: cpinto@ast.cam.ac.uk

of a sample of cool objects by Sanders & Fabian (2011) and more recently in individual elliptical galaxies by our group (Pinto et al. 2014), but in most cases their fluxes are lower than those predicted by cooling flow models. There is an overall deficit of cool ( $\lesssim 0.5$  keV or  $\lesssim 6 \times 10^6$  K) gas in the cores of clusters of galaxies and nearby elliptical galaxies.

Several energetic phenomena are occurring in the cores and in the outskirts of clusters of galaxies and isolated galaxies such as feedback from active galactic nuclei (AGN, see e.g. Churazov et al. 2000; McNamara & Nulsen 2007; Fabian 2012). Briefly, energetic AGN outflows drive turbulence in the surrounding ICM, which then dissipates and heats the ICM balancing the cooling (see e.g. Zhuravleva et al. 2014). AGN can also heat the surrounding gas via dissipation of sound waves (see e.g. Fabian et al. 2003, 2005). The phenomenology can be more complex because galactic mergers and sloshing of gas within the gravitational potential also produce high turbulence (see e.g. Ascasibar & Markevitch 2006; Lau et al. 2009).

In this work we study the coolest X-ray emitting gas in clusters and groups of galaxies and in elliptical galaxies, which is crucial to understand the ICM cooling from  $10^8$  K down to  $10^4$  K. We use high quality archival data and new observations taken with the high-resolution Reflection Grating Spectrometer (RGS) aboard XMM-Newton. We search for a relationship between the cool O VII gas and the turbulence, evidence of resonant scattering and charge exchange in the ICM where neutral gas is observed. We present the data in Sect. 2 and the spectral modeling in Sect. 3. We discuss the results in Sect. 4 and give our conclusions in Sect. 5.

## 2 THE DATA

The observations used in this paper are listed in Table 1. Most objects were already included in our recent work (Pinto et al. 2015), but here we only focus on those which exhibit cool gas producing Fe XVII emission lines. The original catalog, also known as the CHEERS sample, consists of 44 nearby, bright clusters and groups of galaxies and elliptical galaxies with a  $\gtrsim 5\sigma$  detection of the O VIII 1s–2p line at 19 Å and with a well-represented variety of strong, weak, and non cool-core objects. In addition to the CHEERS sources exhibiting Fe XVII emission, here we include two cool objects: NGC 1332 and IC 1459. In NGC 1332, O VIII was detected just below  $5\sigma$ , however its Fe XVII emission lines are much stronger. IC 1459 data were enriched by  $\sim 120$  ks new data awarded during the AO-14. In total we have 24 sources.

The XMM-Newton satellite is provided with two main X-ray instruments: RGS and EPIC (European Photon Imaging Camera). We have used RGS data for the spectral analysis and EPIC (MOS 1 detector) data for imaging. The RGS spectrometers are slitless and the spectral lines are broadened by the source extent. We correct for spatial broadening through the use of EPIC/MOS 1 surface brightness profiles. We repeat the data reduction as previously done in Pinto et al. (2015), but with newer calibration files and software versions (available by January, 2016). All the observations have been reduced with the XMM-Newton Science Analysis System (SAS) v14.0.0. We correct for contamination from soft-proton flares with the standard procedure.

The sources in our sample span a large range of dis-

tances (Table 1). Therefore, we tried to extract spectra in slices with widths of the same physical size. Before choosing an absolute scale, we have tested several extraction regions. For the nearby objects, such as NGC 4636 which is the nearest X-ray bright giant elliptical galaxy, we adopted a width of about  $0.8'$  ( $\sim 4$  kpc) because it provides a good coverage of the inner Fe XVII bright core, strengthens the Fe XVII lines with respect to those produced by the hotter gas phase, and maximizes the detection of the O VII emission lines. The spectra of all objects were then extracted in regions centered on the Fe XVII emission peak with widths scaled by the ratio between the distance of the objects and that of NGC 4636. For NGC 507, 533, 3411 and 4325 we had to adopt a slightly larger width because it was the minimum to provide enough statistics in the Fe XVII lines. The spectra extracted in these regions of approximately equal physical size have been used to measure the Fe XVII line ratios. Finally, we have also extracted spectra in different regions, with widths up to  $3.4'$  which is the RGS sensitive field of view, to improve the O VII detection.

We subtracted the model background spectrum, which is created by the standard RGS pipeline and is a template background file based on the count rate in CCD 9. The spectra were converted to SPEX<sup>1</sup> format through the SPEX task *trafo*. We produced MOS 1 images in the 8–27 Å wavelength band and extracted surface brightness profiles to model the RGS line spatial broadening with the following equation:  $\Delta\lambda = 0.138 \Delta\theta \text{ Å}$  (see the XMM-Newton Users Handbook).

## 3 SPECTRAL ANALYSIS

### 3.1 Baseline model

Our analysis focuses on the 8–27 Å first and second order RGS spectra. We perform the spectral analysis with SPEX version 3.00.00. We scale elemental abundances to the proto-Solar abundances of Lodders & Palme (2009), which are the default in SPEX, use C-statistics and adopt  $1\sigma$  errors.

We have described the ICM emission with an isothermal plasma model of collisional ionization equilibrium (*cie*). The basis for this model is given by the mekal model, but several updates have been included (see the SPEX manual). Free parameters in the fits are the emission measure  $Y = n_e n_H dV$ , the temperature  $T$ , and the abundances (N, O, Ne, Mg, and Fe). Nickel abundance was coupled to iron. Most objects required two *cie* components (see Table 1). Here, we coupled the abundances of the two *cie* components and assumed that the gas phases have the same abundances because the spectra do not allow us to measure them separately. The *cie* emission models were corrected for redshift, Galactic absorption, see Table 1, and line-spatial-broadening through the multiplicative *lpro* component that receives as input the MOS 1 surface brightness profile (see Sect. 2).

We do not explicitly model the cosmic X-ray background in the RGS spectra because any diffuse emission feature would be smeared out into a broad continuum-like component. For several objects, including the Perseus and Virgo clusters, we have added a further power-law emission component to account for any emission from the central AGN

<sup>1</sup> www.sron.nl/spex

**Table 1.** XMM-Newton/RGS observations used in this paper, extraction regions and O VII detection.

Source	t <sup>(a)</sup> (ks)	d <sup>(b)</sup> (Mpc)	W <sup>(b)</sup> (')	CIE <sup>(c)</sup> (Nr)	< kT > <sup>(c)</sup> (keV)	N <sub>H</sub> <sup>(d)</sup> (10 <sup>20</sup> cm <sup>-2</sup> )	R <sub>(f/r) Fe</sub> <sup>(e)</sup>	W(O VII) <sup>(e)</sup> (')	P(O VII) <sup>(e)</sup> (σ)
A 262 (NGC 708)	172.6	63.7	0.20	2	1.19 ± 0.02	7.15	1.91 ± 0.89	—	—
Centaurus (A 3526)	152.8	51.2	0.25	2	1.17 ± 0.02	12.2	1.53 ± 0.22	0.4	3.0
Fornax (NGC 1399)	123.9	17.8	0.72	2	1.21 ± 0.03	1.56	1.27 ± 0.18	—	—
Perseus (A 426)	162.8	72.3	0.18	2	2.71 ± 0.15	20.7	4.30 ± 2.10	0.8	2.7
Virgo (M 87)	129.0	16.6	0.77	2	2.05 ± 0.05	2.11	1.68 ± 0.19	—	—
HCG 62 (NGC 4761)	164.6	66.1	0.24	2	0.85 ± 0.01	3.76	1.57 ± 0.21	—	—
IC 1459	145.4	24.0	0.53	2	0.59 ± 0.04	1.16	1.90 ± 0.65	3.4	3.3
M 49 (NGC 4472)	81.4	15.8	0.81	2	0.88 ± 0.01	1.63	1.70 ± 0.20	—	—
M 84 (NGC 4374)	91.5	16.7	0.77	2	0.83 ± 0.07	3.38	1.86 ± 0.17	0.6	4.1
M 86 (NGC 4406)	63.5	16.1	0.80	2	0.84 ± 0.05	2.97	2.12 ± 0.29	3.4	5.5
M 89 (NGC 4552)	29.1	16.0	0.80	1	0.62 ± 0.08	2.96	1.62 ± 0.25	3.4	3.1
NGC 507	94.5	59.6	0.25 <sup>f</sup>	2	1.06 ± 0.02	6.38	1.59 ± 0.67	—	—
NGC 533	34.7	61.6	0.25 <sup>f</sup>	2	0.87 ± 0.03	3.38	2.36 ± 1.04	—	—
NGC 1316	165.9	19.3	0.66	2	0.70 ± 0.02	2.56	1.90 ± 0.25	0.8	6.9
NGC 1332	63.9	22.9	0.56	2	0.66 ± 0.03	2.42	3.01 ± 0.80	—	—
NGC 1404	29.2	19.2	0.67	2	0.69 ± 0.01	1.57	2.06 ± 0.25	0.6	2.6
NGC 3411	27.1	79.1	0.25 <sup>f</sup>	1	0.93 ± 0.02	4.55	1.24 ± 0.36	—	—
NGC 4261	134.9	29.9	0.43	1	0.71 ± 0.01	1.86	1.60 ± 0.28	—	—
NGC 4325	21.5	112	0.25 <sup>f</sup>	2	0.89 ± 0.02	2.54	1.22 ± 0.32	—	—
NGC 4636	102.5	16.0	0.80	2	0.72 ± 0.01	2.07	1.95 ± 0.09	3.4	5.0
NGC 4649	129.8	16.6	0.77	1	0.90 ± 0.01	2.23	1.27 ± 0.20	—	—
NGC 5044	127.1	35.8	0.36	2	0.89 ± 0.01	6.24	1.44 ± 0.22	—	—
NGC 5813	146.8	29.2	0.44	2	0.68 ± 0.01	6.24	2.61 ± 0.43	3.4	3.2
NGC 5846	194.9	26.9	0.48	2	0.74 ± 0.01	5.12	1.67 ± 0.35	0.8	3.7

<sup>(a)</sup> RGS net exposure time. <sup>(b)</sup> Source distance (average value taken from the Ned database: <https://ned.ipac.caltech.edu/>) and width of the extraction region. <sup>(c)</sup> Number of thermal components and best-fit temperature for a single isothermal model (see Sect. 3.4).

<sup>(d)</sup> Hydrogen column density (see <http://www.swift.ac.uk/analysis/nhtot/>). <sup>(e)</sup> Fe XVII line ratio, width (W) of the region that maximizes the O VII detection and O VII cumulative significance (P) with “—” referring to significance below 99% (see Sect. 3.2).

<sup>(f)</sup> For these objects we had to adopt a larger width for the extraction region to obtain enough statistics in the Fe XVII lines.

(see Russell et al. 2013 and references therein). This is not convolved with the spatial profile because it is produced by a point source. For each source, we have simultaneously fitted the spectra of individual observations by adopting the same model, apart from the emission measures of the *cie* components which were uncoupled to account for the different roll angles of the observations.

We have successfully applied this multi-temperature model to the RGS spectra. However, as previously shown in Pinto et al. (2015), the model underestimates the 17 Å Fe XVII line peaks and overestimates its broadening for some sources, e.g. Fornax, M 49, M 86, NGC 4636, and NGC 5813. This is due to the different spatial distribution of the gas responsible for the cool Fe XVII emission lines and that producing most of the high-ionization Fe-L and O VIII lines. The Fe XVII gas is indeed to be found predominantly in the cores showing a profile more peaked than that of the hotter gas. The spatial profiles estimated with MOS1 images strongly depend on the emission of the hotter gas due to its higher emission measure and therefore they overestimate the spatial broadening of the 15–17 Å lines. It is difficult to extract a spatial profile for these lines because MOS1 has a limited spectral resolution and the images extracted in such a narrow band will lack the necessary statistics (see e.g. Sanders & Fabian 2013). The 17 Å / 15 Å line ratio is also affected by resonant scattering (see e.g. Gilfanov et al. 1987;

Sanders et al. 2008), which requires a different approach. In Sect. 3.3 and 3.4 we account for the different location of the different phases and the Fe XVII (and O VII) resonant scattering.

### 3.2 Search for O VII

Following Pinto et al. (2014), we have removed the O VII ion from the model and fitted two delta lines fixed at 21.6 Å and 22.1 Å, which reproduce the O VII resonance and forbidden lines, respectively. The intercombination line at 21.8 Å is generally weak or insignificant and blends with the resonance line. These lines are corrected by the redshift, the Galactic absorption, and the spatial line broadening as done for the *cie* models. If the resonant line was comparable or stronger than the forbidden lines, we have determined the O VII total significance by fixing the resonance-to-forbidden line flux ratio to  $(r/f) = 1.3$  as predicted by the thermal model. Otherwise the O VII total significance was calculated as the squared-sum of the significance of each line. The latter refers to Perseus, M 89, and NGC 4636 and 5813. We applied this technique to spectra extracted in regions of different widths in order to search for that one maximizing the O VII detection. We adopt as threshold for the O VII detection the 99% confidence level because the objects are distributed in two subsamples with detection levels < 2.0σ and

$> 2.6\sigma$  showing a gap in between. The results are reported in Table 1 and discussed in Sect. 4.

### 3.3 The location of the cool gas

It is possible to probe the extent of the cool (OVII – FeXVII) gas by comparing its linewidth to that of the hot (OVIII – FeXVIII+) gas. The dominant line broadening effect in grating spectra is indeed produced by the spatial extent of the source (normally a few  $1000 \text{ km s}^{-1}$ ), which is almost an order of magnitude larger than the thermal + turbulent broadening (few  $100 \text{ km s}^{-1}$ , see e.g. Pinto et al. 2015 and references therein). The turbulence and thermal broadening are not expected to be significantly different between the two phases (see e.g. Pinto et al. 2015). We therefore did the same exercise for the FeXVII emission lines by removing the FeXVII ion from the model and fitting four delta lines fixed at  $15.01 \text{ \AA}$ ,  $15.26 \text{ \AA}$ ,  $16.78 \text{ \AA}$ , and  $17.08 \text{ \AA}$ , which are the main FeXVII transitions. We do not tabulate the significance of the FeXVII lines because they are typically much larger than  $5\sigma$ .

The *lpro* model in SPEX that corrects for the line broadening has an additional scale parameter  $s$ , which allows to fit the width of the spatial broadening by a factor free to vary (see the SPEX manual). We therefore use one *lpro* model to account for the spatial broadening in the *cie* components that produce the high-temperature lines and another *lpro* model to fit the spatial broadening of the low-temperature OVII and FeXVII lines. Averaging between all objects in our sample, we find that the *lpro* scale parameter of the cool gas is half of that measured for the hot gas.

In Fig. 1 we show the RGS spectra of three interesting sources, the Centaurus cluster, M84 and M89 (from top to bottom). Overlaid on the data there are three spectral models: the baseline *cie* model (thick black line), the delta line model for OVII and FeXVII lines adopting the same spatial broadening as the *cie* models (solid green line), and finally the OVII and FeXVII lines with the spatial scale parameter  $s$  free to vary (dashed red line). In order to better visualize the effect on the fit from spatial broadening, we calculate the ratios from the best-fit models obtained with the delta lines and the best-fitting *cie* model and display them in the bottom panel of each figure. The color is coded similarly to the top panel: the green line is the ratio between the OVII–FeXVII delta model and the *cie* components (with the same spatial broadening); the red line shows the same ratio but with a different spatial broadening. The blue dotted lines show the  $1\sigma$  uncertainties.

The FeXVII lines appear clearly narrower than the hot-gas lines in the Centaurus cluster (A3526), even taking into account the slightly different thermal broadening, but there is no significant wavelength shift (in agreement with Sanders et al. 2008). This suggests that the FeXVII cool ( $\sim 6 \times 10^6 \text{ K}$ ) gas peaks in the central regions and has a smaller extent than that of the hot gas responsible for the OVIII at  $19 \text{ \AA}$  and the higher-ionization FeXX+ ( $\gtrsim 10^7 \text{ K}$ ) lines between  $11 - 13 \text{ \AA}$ . A similar trend is observed in Fornax, M49, M84, NGC 4636–5044–5813, and Perseus. The M84 and M89 elliptical galaxies, whose spectra are dominated by the FeXVII lines, show an OVII excess with respect to the two-phase *cie* model. Interestingly, in M84 (and NGC 5846) the OVII resonant line at  $21.6 \text{ \AA}$  is in excess, while in M89 (and NGC 4636) the excess is shown by

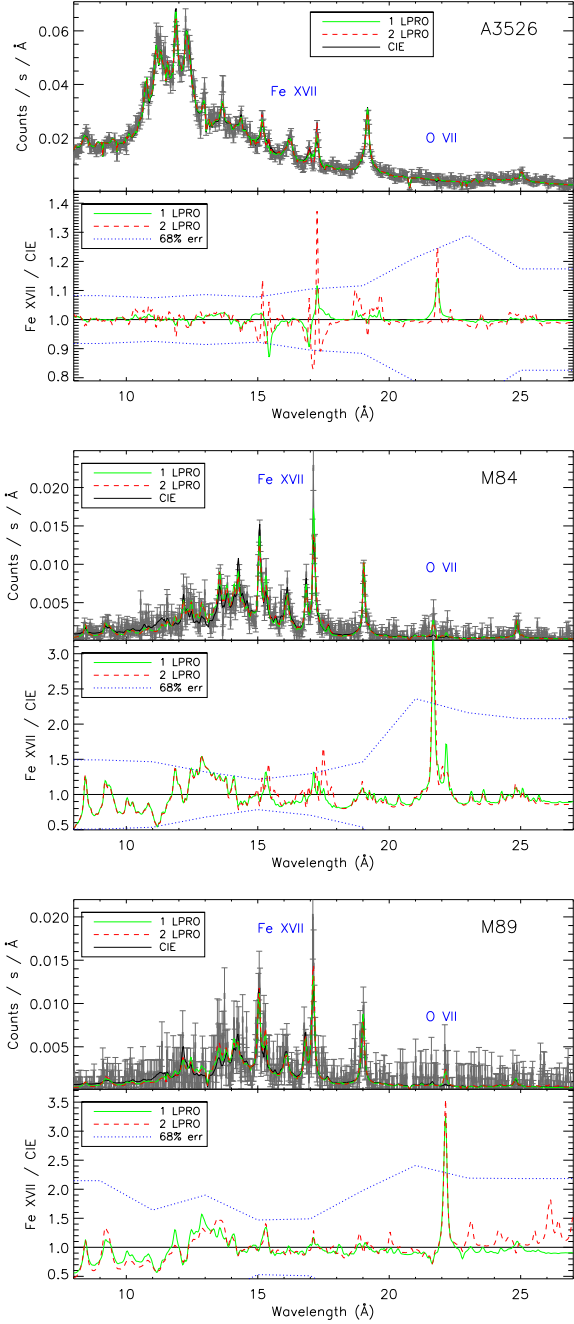


**Figure 1.** From top to bottom: RGS spectra of the Centaurus cluster, M84, and M89. Three spectral models are overlaid: 2-*cie* model (thick black line), delta-line FeXVII model (thick green line) and different spatial broadening (dashed red line). The bottom panels show the ratios between the FeXVII line models and the 2-*cie* model. The blue dotted lines show the  $1\sigma$  uncertainties.

the forbidden line at  $22.1 \text{ \AA}$ . The quality of the spectra of the other objects is not good enough to detect OVII in excess to that already produced by the two-*cie* model. A stronger forbidden line may indicate resonant scattering for both OVII and FeXVII lines as we previously suggested in Pinto et al. (2014).

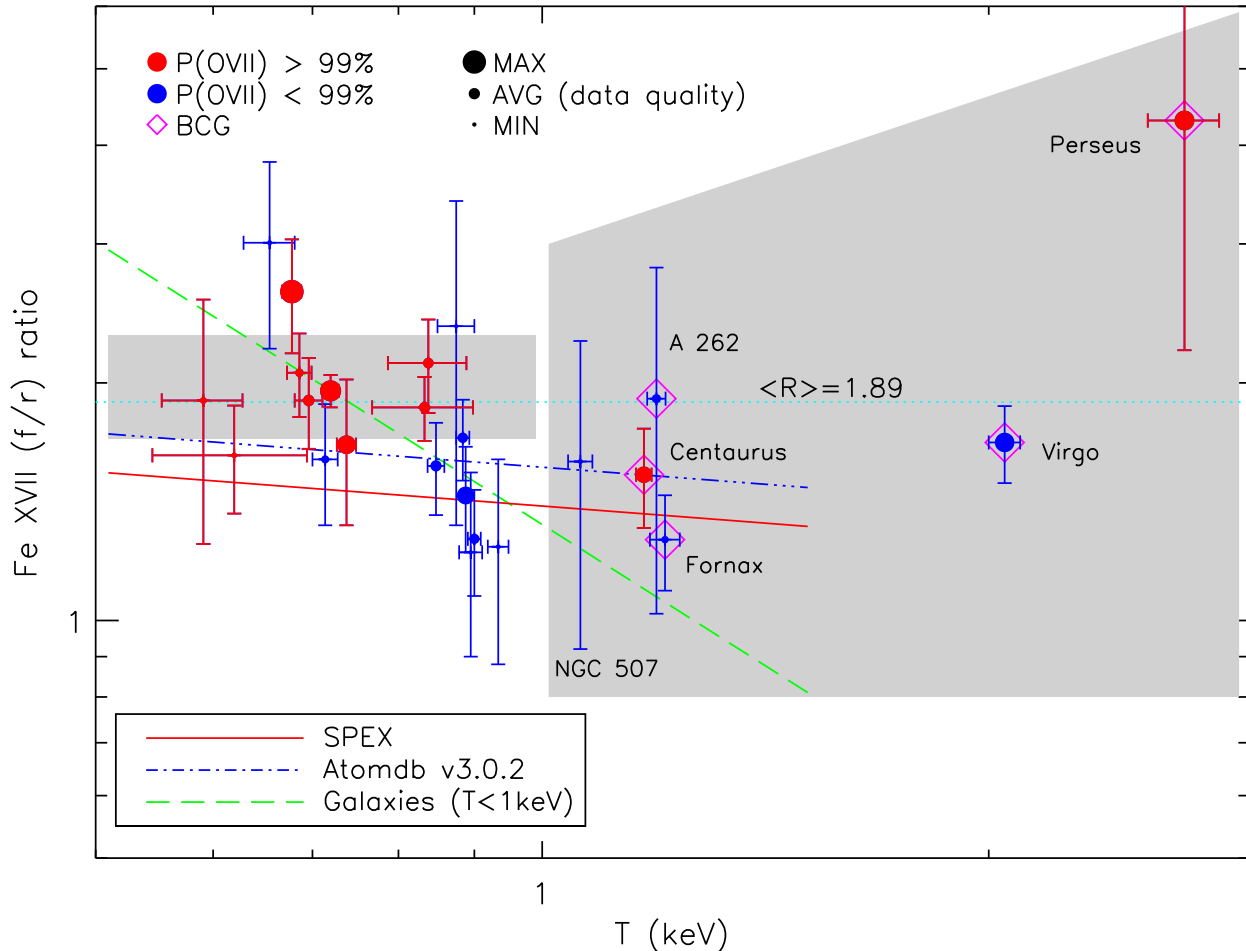


**Figure 2.** Fe XVII forbidden-to-resonance line ratio versus average temperature. O VII detections are reported with red points. The dashed green line shows the best fit in the log-log space for the objects below 1 keV. The theoretical predictions from SPEX and Atomdb v3.0.2 are also shown. The objects above 1 keV are grey-shaded because there is little Fe XVII at those average temperatures and most of it should be produced by a cooler phase. The small grey box shows the average Fe XVII ratio ( $2.00 \pm 0.29$ ) of the elliptical galaxies below 1 keV with O VII detected above the 99% confidence level.

### 3.4 O VII VS Turbulence

When turbulence is low the resonant line can be optically thick; it is therefore absorbed and re-emitted in a random direction with the line being suppressed towards the bright core and enhanced outside. This does not occur at high turbulence due to the energy shift of the transitions (see e.g. Werner et al. 2009 and de Plaa et al. 2012). The forbidden lines have a smaller oscillator strength and are much less affected. It is then interesting to measure the Fe XVII line resonant scattering of the sources in our sample, which is an indicator of (low-) turbulence, and compare it to the O VII detection, in a certain temperature range.

We have used the Fe XVII line fluxes measured in Sect. 3.3 to calculate the Fe XVII (f/r) line ratios for the models with a different spatial broadening between these lines and the hot gas, and quote the results in Table 1. In order to estimate an average temperature for each source, we fit again the RGS spectra with only one single *cie* component. The average temperatures estimated through these models are quoted in Table 1.

We plot the Fe XVII (f/r) line ratios versus the temperature in Fig. 2 with the red points showing the sources with

O VII detection above the 99% confidence level. The point size scales with the average S/N ratio of the RGS spectra at 17 Å. We also show the Fe XVII line ratios as predicted by a thermal model without resonant scattering according to the Atomdb v3.0.2 and SPEX to visualize the strength of the resonant scattering in each source and the systematic uncertainties in the atomic data. Points below the theoretical predictions would be unphysical because it is difficult to strengthen only the resonant line in the line-of-sight towards the center of the galaxies (although charge-exchange can slightly enhance the Fe XVII resonant line). All our Fe XVII (f/r) line ratios agree with the theoretical predictions or are above the theoretical curves, indicating moderate resonant scattering and therefore low-to-mild (subsonic) turbulence. We fit a straight-line in the log-log space for the objects with  $T < 1$  keV, and found a significant anti-correlation between the Fe XVII (f/r) line ratio and the average temperature (well above the  $3\sigma$  confidence level,  $p$ -value = 0.00026, with slope  $-0.79 \pm 0.18$ , see the green dashed line in Fig. 2). This may indicate either a decrease in optical depth or an increase in turbulence or both. We caution against the comparison with the brightest cluster galaxies (BCG), i.e. those in A 262, Centaurus, Fornax, Perseus, and Virgo clusters,

because above 1 keV the ICM becomes optically thin to the Fe XVII emitted by the cooler gas phases ( $kT < 0.9$  keV) and therefore resonant scattering becomes insensitive to turbulence in the cores of these systems. All results are discussed in Sect. 4.

### 3.5 Systematic effects

There are several systematics that may affect our results and their interpretation such as the background subtraction, the line blending and the uncertainties in the atomic database.

The model background spectra used throughout this work adopt long exposures of blank fields. This is a safe approach since any background contribution to the weak O VII or the strong Fe XVII lines would be smeared out in a continuum like feature. For some bright and compact objects such as NGC 1316–1404 M 89 we could extract a background spectrum in the outer regions of the RGS detector and match it with the model background spectrum. The spectra were comparable and no significant difference in the line ratios were found. We also tested a different continuum with a local (14.5–18.0 Å) fit using a power-law and a few delta lines obtaining larger statistical uncertainties and consistent results with the previous Fe XVII measurements. We tested a power-law continuum for the 19.5–22.5 Å range obtaining similar O VII detections.

We have also checked the effects of blending with other lines. The O VII resonant and forbidden lines are located in a rather clean spectral range apart from O VI and O VII intercombination lines. As mentioned in Sect. 1, there are only small amounts of O VI in these objects as clearly shown in far-UV spectra. The O VI stronger line at 22.0 Å is also expected to be resolved by RGS due to the smaller extent, and therefore line broadening, of the O VI–VII cool phases. The O VII intercombination line is 5.5 weaker than the resonant line and also not expected to significantly affect our results. The Fe XVII resonant and forbidden lines are in a crowded spectral region, but they are much stronger than the neighbor lines. We have artificially doubled the flux of the brightest neighbor lines, which is more than the statistical uncertainties. The Fe XVII (f/r) line ratio was consistent with the standard measurements.

The uncertainties in the atomic database do not affect our measurements of line ratios, but of course the interpretation of resonant scattering. There is a significant ( $> 20\%$ ) difference between the Fe XVII (f/r) line ratio as predicted by AtomDB and SPEX. This means that we do not know the absolute value of resonant scattering in our sources, which is crucial to estimate the absolute scale of turbulence, but the relative differences between line ratios measured in different objects should not be highly affected.

## 4 DISCUSSION

In Sect. 3.2 we have searched for O VII ( $\sim 2 \times 10^6$  K) gas in a sample of 24 objects, including clusters and groups of galaxies and elliptical galaxies, with strong ( $> 5\sigma$ ) Fe XVII line emission. We have detected O VII above the 99% confidence level in 11 sources and shown that O VII is preferably found in the cores of the sources, possibly following the distribution of the Fe XVII ( $> 5 \times 10^6$  K) gas. Exceptions are

IC 1459 and M 89 where the lower count rate requires to integrate photons over a larger region. For M 86, NGC 4636 and NGC 5813 the O VII is also better detected in the wider slit most likely due to their more extended cool cores.

In order to search for a link between cooling and turbulence, we have plotted the Fe XVII forbidden-to-resonant line ratio with the temperature and the O VII significant detections in Fig. 2. The high quality data points show some evidence for O VII to be mainly detected in sources with significant resonant scattering, which indicates the low level of turbulence. Although our sample is incomplete and the resonant scattering is more sensitive at lower temperatures, our results are consistent with a picture where turbulence is heating the gas and preventing it to cool below  $\sim 0.45$  keV, where O VII line emission begins to be important.

### 4.1 O VII charge exchange or scattering?

At temperatures of 0.2-to-0.6 keV the O VII resonance-to-forbidden line ratio is predicted to be between 1.25–1.35. We found (r/f) line ratios lower than 1.25 in the RGS spectra of NGC 4636, M 89, and NGC 1404 as already shown in Pinto et al. (2014). Our values could be due to either suppression of the resonant line via resonant scattering or enhancement of the forbidden line by photoionization or charge exchange.

The O VII resonance line at 21.6 Å may be subject to resonant scattering. At the temperature of  $\sim 0.5$  keV, where the Fe XVII ionic concentration peaks, the O VII is optically thin and no longer self-absorbed along the line-of-sight. However, it is possible that the gas is distributed in various non-volume filling phases at different temperatures. We multiplied the two *cie* emission components for a collisionally-ionized absorbing model (*hot* model in SPEX) and re-fit the RGS spectrum of NGC 4636. We obtained a column density of  $1.24 \pm 0.30 \times 10^{20} \text{ cm}^{-2}$  with a temperature of  $0.23 \pm 0.03$  keV, which is lower than the  $0.43 \pm 0.07$  keV value measured for the *cie* component responsible for the O VII emission. The presence of such cool gas is suggested by the detection of a large amount of H $\alpha$  emission in the core of NGC 4636 (Werner et al. 2014). It is suspicious, however, that the absorbing gas is cooler than the emitting gas despite the need to be located (on average) in outer regions where higher temperatures are expected unless the cool gas is clumpy.

The astrophysical processes that strengthen the O VII forbidden line emission are photoionization and charge exchange. We can rule out photoionization because no bright AGN is observed in NGC 4636. Charge exchange (CX hereafter) occurs when ions interact with neutral atoms or molecules; one or more electrons are transferred to the ion into an excited state, which decays and emits a cascade of photons increasing the forbidden-to-resonance ratios of triplet transitions. This process is often observed in supernova remnants (e.g. Puppis A, Katsuda et al. 2012), starburst galaxies (e.g. M 82, Liu et al. 2011) and colliding stellar winds (e.g. Solar Wind, Snowden et al. 2004).

The CX plasma code recently provided by Gu et al. (2016) is implemented in SPEX v3.00.00 (*cx* model). Gu et al. (2015) first used this code to successfully describe the unidentified 3.5 keV feature in the lower resolution CCD spectrum of the Perseus cluster. We re-fit the NGC 4636

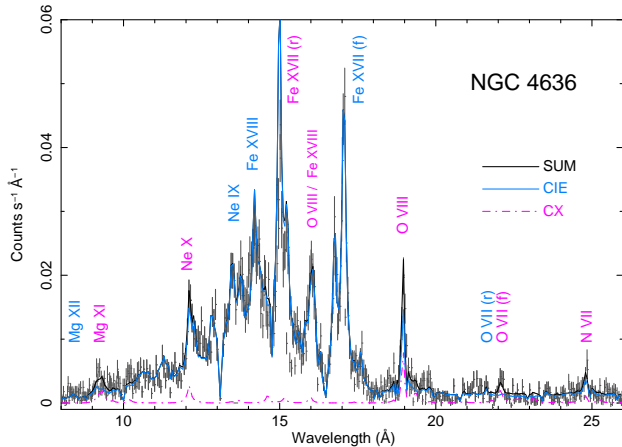


**Figure 3.** NGC 4636 RGS first order spectrum with hybrid model consisting of isothermal and charge-exchange components.

spectrum with a new *cie* (driven by the Fe XVII–XVIII lines) + *cx* (mainly, O VII–VIII, Ne X, and Mg XI) model corrected by redshift and Galactic absorption and obtain results comparable to the resonant scattering (*hot*) model described above. In the fit we exclude the 13.8–15.5 Å spectral range because it contains several Fe XVII lines suppressed by resonant scattering which would lead to a wrong estimate of the temperature. In Fig. 3 we show the best fit with the contribution from the *cie* and *cx* components. Charge exchange provides a reasonable description of the O VII lines and produces significant O VIII, Ne X, and Mg XI emission and accounts for  $\sim 10\%$  of the flux in the 0.3–2.0 keV energy band.

The ionic temperature of the *cx* component was coupled to the  $\sim 0.7$  keV temperature of the *cie* component. If left free to vary, a better fit provides  $T_{\text{ion}} = 0.40 \pm 0.05$  keV, in agreement with the 2-*cie* model, which may suggest that the charge exchange is occurring between neutrals and the cooler O VII phase rather than the hotter gas phase associated with the Fe XVII lines. This may indicate that the cool O VII gas is a better tracer of the cold neutral phase and that they could be somewhat cospatial, both distributed in clumps. The CX code calculates velocity-dependent rates with which we measure a collision velocity lower than  $50 \text{ km s}^{-1}$  (at 68% level), in agreement with the low turbulence found in NGC 4636 (Werner et al. 2009). This is the first time that a charge exchange model is successfully applied to a high-resolution X-ray spectrum of a giant elliptical galaxy.

#### 4.2 Resonant scattering in Perseus?

In Fig. 2 we have shown that the Perseus cluster has an unexpected, high ( $4 \pm 2$ ), Fe XVII (f/r) line ratio. The spectrum extracted within a larger region of width  $\sim 0.8'$  (see Fig. 4) holds much smaller error bars and constrains Fe XVII (f/r)  $\geq 4$ . This value is higher than that measured in any other object and remarkable if compared to the other clusters (A 262, Centaurus, Fornax and Virgo). The inner core of the Perseus cluster is dominated by a hot  $\sim 3$  keV plasma, but it has been clearly shown to be multiphase with the inner arcminute ( $\sim 20$  kpc) having significant emission from 0.5–4 keV (see e.g. Sanders & Fabian 2007).

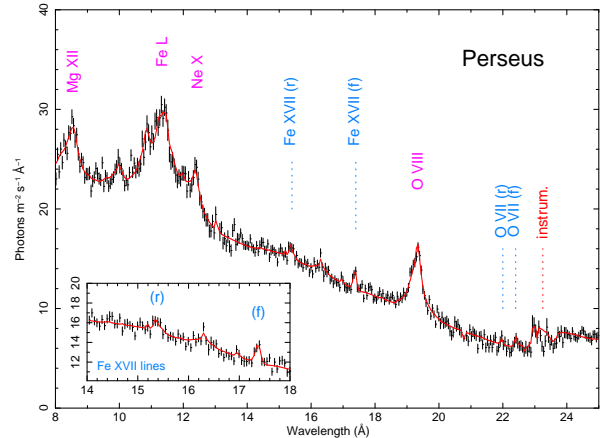


**Figure 4.** Perseus RGS first order spectrum with multiphase thermal emission model absorbed by isothermal gas at 0.6 keV.

Below 1 keV and in a low-turbulence regime the 15 Å resonance line is optically thick and it may therefore be subject to resonant scattering in the line-of-sight. We have therefore re-fitted the Perseus spectrum multiplying the two thermal components by a collisionally-ionized absorption model (*hot* model) to test the suppression of the Fe XVII resonant line (as previously done for the O VII lines in NGC 4636 in Sect. 4.1). We have ignored the first order spectra between 10 and 14 Å due to high pile up and use the second order RGS 1 and 2 spectra because they are not significantly affected by pileup and their statistics peak in this wavelength range. This model reasonably describes the 15–17 Å Fe XVII lines (see Fig. 4) and provides a column density of  $\sim 2 \times 10^{20} \text{ cm}^{-2}$  and a temperature of  $\sim 0.6$  keV.

Fabian et al. (2015) suggested that high-resolution X-ray spectra enable to search for evidence of ICM absorption onto the AGN continuum in NGC 1275, the brightest cluster galaxy in Perseus, with a focus on the hard X-ray band where Fe K lines dominate. We have tested the same approach in the soft RGS band by applying the *hot* absorption model only to the nucleus, which was fitted with a power law; the two *cie* emission line components are only absorbed by the Galactic neutral ISM. This AGN-only absorption model is statistically indistinguishable to the previous one, with  $\Delta\chi^2$  and  $\Delta\text{C-stat}$  of 6 for 1948 degrees of freedom, but a column density of  $\sim 1.5 \times 10^{21} \text{ cm}^{-2}$  is required, in good agreement with the predictions of Fabian et al. (2015). If the suppression of the 15 Å Fe XVII resonant line and the detection of absorption are interpreted as resonant scattering, which is a very likely scenario, then this means that the cool gas in Perseus is characterized by low turbulence.

## 5 CONCLUSIONS

In this work we have confirmed and extended our previous discovery of O VII emission lines in spectra of elliptical galaxies as well as groups and clusters of galaxies. This is the coolest X-ray emitting intracluster gas and seems to be connected to the mild Fe XVII gas, being located preferably at small (1–10 kpc) scales. The O VII is often detected in objects with strong resonant scattering of photons in the Fe XVII lines, indicating subsonic turbulence. This would



be consistent with a scenario where cooling is suppressed by turbulence in agreement with models of AGN feedback, gas sloshing and galactic mergers. We note that a larger sample of sources and consequently more observations are needed to better disentangle resonant scattering effects due to temperature and turbulence; the current sample is incomplete. In some objects the OVII resonant line is weaker than the forbidden line either due to resonant scattering or to charge-exchange processes occurring in the gas as we have shown for NGC 4636. The Perseus cluster shows an anomalous, high, Fe XVII forbidden-to-resonance line ratio, which can be explained with resonant scattering by cool gas in the line-of-sight under a regime of low turbulence. In two forthcoming papers (Ogorzalek et al., Pinto et al.) we will compare the measurements of Fe XVII line ratios with those predicted by theoretical models of resonant scattering that take into account thermodynamic properties of these objects in order to estimate the turbulence in both their cores and outskirts. This will provide further insights onto the link between cooling, turbulence, and the phenomena of AGN feedback, sloshing, and mergers occurring in clusters and groups of galaxies.

## ACKNOWLEDGMENTS

This work is based on observations obtained with XMM-Newton, an ESA science mission funded by ESA Member States and USA (NASA). We also acknowledge support from ERC Advanced Grant Feedback 340442 and new data from the awarded XMM-Newton proposal ID 0760870101. Y.Y.Z. acknowledges support by the German BMWi through the Verbundforschung under grant 50OR1506.

## REFERENCES

- Ascasibar, Y. & Markevitch, M. 2006, *ApJ*, 650, 102
- Bregman, J. N., Fabian, A. C., Miller, E. D., & Irwin, J. A. 2006, *ApJ*, 642, 746
- Bregman, J. N., Miller, E. D., Athey, A. E., & Irwin, J. A. 2005, *ApJ*, 635, 1031
- Churazov, E., Forman, W., Jones, C., & Böhringer, H. 2000, *A&A*, 356, 788
- de Plaa, J., Zhuravleva, I., Werner, N., et al. 2012, *A&A*, 539, A34
- Fabian, A. C. 1994, *ARA&A*, 32, 277
- Fabian, A. C. 2012, *ARA&A*, 50, 455
- Fabian, A. C., Reynolds, C. S., Taylor, G. B., & Dunn, R. J. H. 2005, *MNRAS*, 363, 891
- Fabian, A. C., Sanders, J. S., Allen, S. W., et al. 2003, *MNRAS*, 344, L43
- Fabian, A. C., Walker, S. A., Pinto, C., Russell, H. R., & Edge, A. C. 2015, *MNRAS*, 451, 3061
- Gilfanov, M. R., Syunyaev, R. A., & Churazov, E. M. 1987, *Soviet Astronomy Letters*, 13, 3
- Gu, L., Kaastra, J., & Raassen, A. J. J. 2016, *ArXiv e-prints*
- Gu, L., Kaastra, J., Raassen, A. J. J., et al. 2015, *A&A*, 584, L11
- Katsuda, S., Tsunemi, H., Mori, K., et al. 2012, *ApJ*, 756, 49
- Lau, E. T., Kravtsov, A. V., & Nagai, D. 2009, *ApJ*, 705, 1129
- Liu, J., Mao, S., & Wang, Q. D. 2011, *MNRAS*, 415, L64
- Lodders, K. & Palme, H. 2009, *Meteoritics and Planetary Science Supplement*, 72, 5154
- McNamara, B. R. & Nulsen, P. E. J. 2007, *ARA&A*, 45, 117
- Peterson, J. R., Kahn, S. M., Paerels, F. B. S., et al. 2003, *A&A*, 590, 207
- Pinto, C., Fabian, A. C., Werner, N., et al. 2014, *A&A*, 572, L8
- Pinto, C., Sanders, J. S., Werner, N., et al. 2015, *A&A*, 575, A38
- Russell, H. R., McNamara, B. R., Edge, A. C., et al. 2013, *MNRAS*, 432, 530
- Sanders, J. S. & Fabian, A. C. 2007, *MNRAS*, 381, 1381
- Sanders, J. S. & Fabian, A. C. 2011, *MNRAS*, 412, L35
- Sanders, J. S. & Fabian, A. C. 2013, *MNRAS*, 429, 2727
- Sanders, J. S., Fabian, A. C., Allen, S. W., et al. 2008, *MNRAS*, 385, 1186
- Snowden, S. L., Collier, M. R., & Kuntz, K. D. 2004, *ApJ*, 610, 1182
- Werner, N., Oonk, J. B. R., Sun, M., et al. 2014, *MNRAS*, 439, 2291
- Werner, N., Zhuravleva, I., Churazov, E., et al. 2009, *MNRAS*, 398, 23
- Zhuravleva, I., Churazov, E., Schekochihin, A. A., et al. 2014, *Nature*, 515, 85

This paper has been typeset from a  $\text{\LaTeX}$  file prepared by the author.